A NUMERICAL STUDY ON CONVECTION AROUND A SQUARE CYLINDER USING AL_2O_3-H_2O NANOFLUID

by

Mohammad Sadegh VALIPOUR [a], Reza MASOODI [b*], Saman RASHIDI [a], Masoud BOVAND [c], and Mojtaba MIRHOSSEINI [c]

[a] Department of Mechanical Engineering, Semnan University, Semnan, Iran
[b] School of Design and Engineering, Philadelphia University, Philadelphia, Penn., USA
[c] Department of Mechanical Engineering, Semnan Branch, Islamic Azad University, Semnan, Iran

Original scientific paper
DOI: 10.2298/TSCI121224061V

In this paper, a numerical simulation has been performed to study the fluid flow and heat transfer around a square cylinder utilizing AL_2O_3-H_2O nanofluid over low Reynolds numbers. Here, the Reynolds number is varied within the range of 1 to 40 and the volume fraction of nanoparticles (φ) is varied within the range of $0 < \varphi < 0.05$. Two-dimensional and steady mass continuity, momentum, and energy equations have been discretized using finite volume method. SIMPLE algorithm has been applied for solving the pressure linked equations. The effect of volume fraction of nanoparticles on fluid flow and heat transfer were investigated numerically. It was found that at a given Reynolds number, the Nusselt number, drag coefficient, re-circulation length, and pressure coefficient increases by increasing the volume fraction of nanoparticles.

Key words: *nanofluids, finite volume, square cylinder, Reynolds number, volume fraction*

Introduction

Convective heat transfer can be enhanced by using various methods and techniques, such as increasing the effective heat transfer surface or the heat transfer coefficient. Convection may be used in the local cooling, which is one of the most important technical problems facing many industrial applications. Some of the important applications of convective cooling are microelectronics, transportation, nuclear power plants, cooling of microchips in computers, and heat exchangers [1]. Recently, a new class of heat transfer fluids, called nanofluids, has been developed by suspending nanocrystalline particles in fluids. These fluids have shown high thermal properties due to order-of-magnitude larger thermal conductivity of solid particles comparing with base liquid.

In recent years, many researches have been performed to study the effects of nanofluid on convective heat transfer rate. Lamura *et al.* [2] investigated the multi-particle collision flow around a circular and a square cylinder. Their results showed that a thermal re-normalization of the viscosity could indeed be responsible for the small deviations of the values for the re-circulation length and the drag coefficient compared to the lattice Boltzmann results. The specific heat

* Corresponding author; e-mail: masoodir@philau.edu

capacity of CuO nanofluid was investigated by Zhou *et al.* [3]. They studied the effects of particle size and particle-liquid interface on the specific heat capacity of nanofluid. They found that discrepancy between nanoparticles with different sizes is small when increasing the nanoparticle volume concentration, which is due to the large specific heat capacity of base fluid. Peng *et al.* [4] measured the specific heat capacity of water based Cu, Al, Al_2O_3, and CuO nanofluids, and propylene glycol-based Al_2O_3 nanofluid. Wong and Castillo [5] surveyed heat transfer mechanisms and clustering in nanofluids. A summary of the recent works on the heat transfer of nanofluids (dilute liquid suspensions of nanoparticles) is reported by Ding *et al*. [6]. Their results showed that natural convective heat transfer coefficient systematically decreases with increasing nanoparticle concentration. Therefore, either enhancement or deterioration can occur in the forced convective heat transfer of nanofluids. The exact reason is unclear, but particle migration is shown to be an important factor [6].

Ellahi *et al*. [7] presented series solutions for magnetohydrodynamic flow of non-Newtonian nanofluid and heat transfer in coaxial porous cylinder with slip conditions. Also in another research, Ellahi *et al.* [8] presented series solutions of non-Newtonian nanofluids with Reynolds' model and Vogel's model by means of the homotopy analysis method. Non-Newtonian nanofluid flow through a porous medium between two coaxial cylinders with heat transfer and variable viscosity was studied by Ellahi *et al.* [9]. The effects of MHD and temperature dependent viscosity on the flow of non-Newtonian nanofluid in a pipe were studied analytically by Ellahi *et al*. [10].

A numerical study on the flow and heat transfer across a confined square cylinder in the steady flow regime has been performed by Dhiman *et al*. [11]. Their results showed that the average Nusselt number increases monotonically with an increment in Reynolds number and/or Prandtl number. Furthermore, as Reynolds number increases, the length of the re-circulation region increases. The Effect of thermal buoyancy on vortex shedding behind a square cylinder has been studied by Chatterjee and Mondal [12]. Also, Yoon *et al.* [13] investigated the flow past a square cylinder with different incidence angles. It was found that for steady flow, the wake length increases with increasing Reynolds number. Another numerical study on the forced convection heat transfer from a rectangular cylinder was performed by Rahnama *et al.* [14]. They found that increasing aspect ratio decreases Nusselt number for all Reynolds numbers. They also found that Nusselt number increases by increasing Reynolds number. Mixed convection inside a rectangular enclosure, filled with nanofluid, was studied by Mahmoodi [15]. Soltanipour *et al.* [16] studied the heat transfer enhancement using γ-Al_2O_3-H_2O nanofluid in a curved duct.

Another numerical study on fluid flow and heat transfer around a solid circular cylinder utilizing nanofluid was done by Valipour and Zare Ghadi [17]. Their results showed that as the solid volume fraction increases, the magnitude of minimum velocity in the wake region and recirculation length increases but separation angle decreases. A study on unconfined nanofluid flow and heat transfer around a square cylinder has been performed by Etminan-Farooji *et al.* [18] recently. They focused on the effects of Peclet number and types of nanofluids on heat transfer from the cylinder rather than fluid flow hydrodynamics. Sarkar *et al.* [19] studied vortex structure distributions and mixed convective heat transfer around a solid circular cylinder utilizing nanofluid for unsteady regime. Their result showed that the Strouhal number increases by increasing solid volume fraction. It also showed that increase in Strouhal numbers leads to reduction in vortex detachment. The core of the vortices grows during subsequent processes of vortex shedding cycle.

Although many researchers studied convective heat transfer around a cylinder using nanofluids but there are still several areas that need more research to enable us understand and use nanofluid convection. One of such problems is convection around a square cylinder using H_2O-Al_2O_3 nanofluid, which is the subject of this paper. Such structure (square cylinder) has many practical applications, such as using square tubes in novel heat exchangers, cooling of electronic components, using square bars as flow dividers to form weld lines in polymer engineering applications, cooling towers, *etc*. The objective of this research is to study the effect of nanofluid on heat transfer rate and other parameters such as drag coefficient, pressure coefficient, length of re-circulation region, and streamlines in laminar regime. To achieve these objectives, we performed a comprehensive numerical study to investigate the laminar forced convection heat transfer around a square cylinder using Al_2O_3-H_2O nanofluid.

Analysis

Governing equations

The mixture model has a behavior similar to single phase model. Therefore, single-phase approach is adapted for nanofluid modeling, in which the dissipation and operating pressure are neglected [20]. To use single-phase approach, ultrafine (<100 nm) solid particles are considered. The governing equations for two dimensional and steady state flow with single phase approach for nanofluid modeling are mass conservation, momentum, and energy equations, as:

$$\nabla(\rho_{\text{eff}} V_m) = 0 \tag{1}$$

$$\nabla(\rho_{\text{eff}} V_m V_m) = -\nabla p + \nabla(\mu_{\text{eff}} \nabla V_m) \tag{2}$$

$$\nabla(\rho_{\text{eff}} C_{\text{eff}} V_m T) = \nabla(k_{\text{eff}} \nabla T) \tag{3}$$

where ρ_{eff}, V_m, p, m_{eff}, C_{eff}, and T are effective density, mixture velocity, pressure, effective viscosity, effective specific heat, and temperature, respectively.

The Brownian motion of nanoparticles has been considered to determine the thermal conductivity and dynamic viscosity of this mixture. In above equations, ρ_{eff} is calculated using the expression:

$$\rho_{\text{eff}} = (1-\varphi)\rho_{\text{f}} + \varphi\rho_{\pi} \tag{4}$$

where φ is volume fraction and f and p denotes fluid and particle, respectively.

The effective specific heat, as defined by Zhou and Ni [21], is:

$$C_{\text{eff}} = \frac{(1-\varphi)\rho_{\text{f}} C_{\text{f}} + \varphi\rho_{\text{p}} C_{\text{p}}}{\rho_{\text{eff}}} \tag{5}$$

where ρ_{eff} is calculated using eq. (4). For mixture dynamic viscosity expression, which is a function of temperature (T), nanoparticle diameter (d_{p} = 30 nm), nanoparticle volume fraction (φ), nanoparticle density (ρ_{p}), and the base-fluid physical properties, as reported by Masoumi *et al*. [22], were used. The nanofluid effective viscosity is defined by Masoumi *et al*. [22] as:

$$\mu_{\text{eff}} = \mu_{\text{f}} + \frac{\rho_{\text{p}} V_{\text{B}} d_p^2}{72 N \delta} \tag{6}$$

where N depends on the base fluid viscosity and the diameter and volume fractions of the nanoparticles and has been calculated by the equation [22]:

$$N = \mu_f^{-1}[(n_1 d_p + n_2)\varphi + (n_3 d_p + n_4)]$$
$$n_1 = -0.000001113, \quad n_2 = -0.000002771, n_3 = 0.00000009, \quad n_4 = -0.000000393 \tag{7}$$

Also in eq.(6), V_B is the Brownian velocity of nanoparticles that depends on temperature, diameter and density of particles and δ – the distance between particles that depends on diameter and volume fractions of the nanoparticles. V_B and δ are defined by [22]:

$$V_B = \frac{1}{d_p}\sqrt{\frac{18K_B T}{\pi \rho_p d_p}} \tag{8}$$

$$\delta = \sqrt[3]{\frac{\pi}{6\varphi}} d_p \tag{9}$$

where K_B is Boltzmann constant (K_B =1.3807·10^{-23} J/K) and d_p – the nanoparticle diameter (30 nm).

The correlation of Chon *et al*. [23], which considers the Brownian motion and mean diameter of the nanoparticles, was used for calculating the effective thermal conductivity:

$$\frac{k_{eff}}{k_f} = 1 + 64.7\varphi^{0.7460}\left(\frac{d_f}{d_p}\right)^{0.3690}\left(\frac{k_s}{k_f}\right)^{0.7476} \mathrm{Pr}^{*0.9955}\ \mathrm{Re}^{*1.2321} \tag{10}$$

where d_f is molecular diameter of base fluid (0.3 nm), k_f – the fluid thermal conductivity, and k_s – the solid thermal conductivity. The Prandtl and Reynolds numbers in eq. (10) are defined as:

$$\mathrm{Pr} = \frac{\mu}{\rho_f \alpha_f} \tag{11}$$

$$\mathrm{Re}^* = \frac{\rho_f K_B T}{3\pi\mu^2 l_{BF}} \tag{12}$$

where l_{BF} is the mean free path of water (l_{BF} = 0.17 nm) and μ can be calculated by [23]:

$$\mu = 2.414 \cdot 10^{-5} \cdot 10^{\frac{247.8}{T-140}} \tag{13}$$

Note that Reynolds number in eq. (12) (Re*) is different than the flow Reynolds number, which was defined in nomenclature section.

Boundary conditions

The flow is assumed to be from the left side (see fig. 1). The entrance boundary conditions are given as:

$$V_{m,x} = V_{in}, \quad V_{m,y} = 0, \quad T_m = T_{in} \tag{14}$$

The relevant boundary condition at the interface between fluid and solid are defined as:

$$V_{m,x} = V_{m,y} = 0, \quad T_w = T_m \tag{15}$$

To minimize the effects of the outer boundaries, the dimensions of the computational domain in the vertical and horizontal directions are defined as 50 times the size of the cylinder (fig. 1). Therefore, computational domain has a dimension 50S × 50S. At the upper and lower boundaries, a frictionless wall and zero heat flux are considered:

$$\frac{\partial V_{\mathrm{m,x}}}{\partial y}=0, \quad V_{\mathrm{m,y}}=0, \quad \frac{\partial T_{\mathrm{m}}}{\partial y}=0 \qquad (16)$$

For outlet boundary, the Neumann boundary condition was considered for both velocity and temperature fields.

Solution technique

The governing equations with the relevant boundary conditions mentioned in previous two subsections, were discretized using finite volume method (FVM). To solve the pressure linked equations, a pressure correction equation, based on SIMPLE iterative algorithm, was used [24]. The second order upwind scheme was used to discretize the convection terms and Green-Gauss method was adopted for discretizing the diffusion terms. To check the convergence of the sequential iterative solution, the maximum relative error in the values of the dependent variables between two successive iterations was set to 10^{-5}. The numerical simulations were done using an in-house code that was adapted and modified to solve this specific problem. We considered specific volume fractions and then solved governing equations to find velocity and temperature fields for each volume fraction.

Grid independence study

Figure 2 shows the wake bubble geometry. As shown in fig. 2, the length of re-circulation region (L_R) is defined as the distance between the end of the wake and the end of the square cylinder. A simple 2-D and square mesh, clustered near the walls and at the interface between fluid and solid, is used here. This mesh is refined near the interface between fluid and solid regions, where the velocity and temperature gradients are large. Figure 3 shows the computational domain and the grids near the interface.

We made a grid independence test by considering several different grid sizes. Table 1 shows the effect of mesh size on the length of re-circulation region (LR) and average Nusselt number for square cylinder when Reynolds number is 20. The numerical results were obtained for four different mesh sizes. By comparing different grid sizes and relevant length of

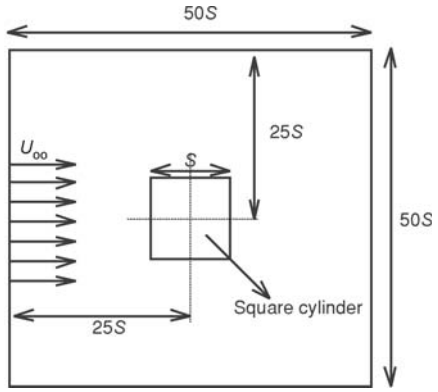

Figure 1. Computational domain and geometry of the cylinder

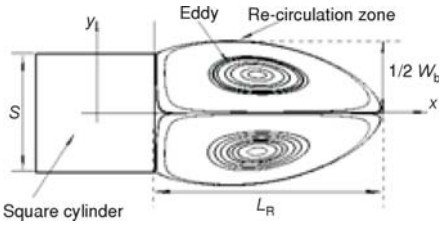

Figure 2. Wake bubble geometry

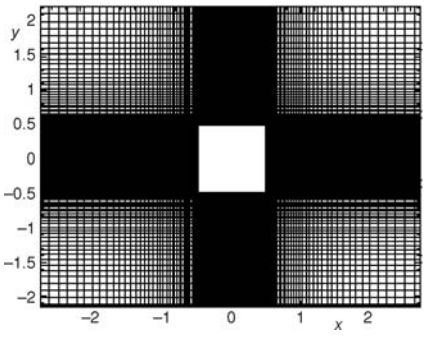

Figure 3. The grid system near the wall

Table1. Effect of grid size on the average Nusselt number and the overall wake length at Re = 20

Cases	Grid size	Nu_{ave}	L_R
1	40 × 40	1.961	1.215
2	80 × 80	2.0201	1.266
3	160 × 160	2.0423	1.298
4	240 × 240	2.0499	1.31

re-circulation region, it was found that the percentage difference of LR and average Nusselt number between the two grids namely, 160 × 160 and 240 × 240, are 0.92% and 0.37%, respectively. Thus, our grid sensitivity study demonstrated that the grid-independent results should be achieved using a 240 × 240 grid for this problem.

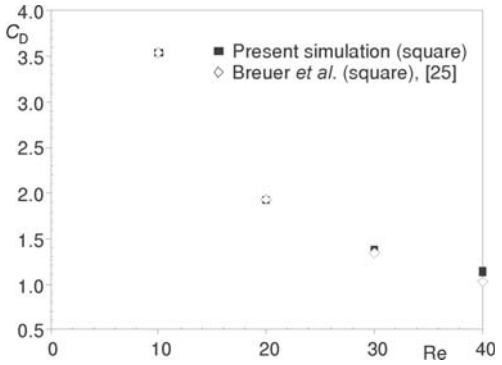

Figure 4. Variation of drag coefficient with Reynolds number for clear fluid

Validation

In order to validate the model and numerical procedure, a comparison of drag coefficient with some available numerical data has been done. Figure 4 shows the drag coefficient on the square cylinder (CD) (for clear fluid) as a function of Reynolds number. It shows that our numerical results compares well with the numerical data of Breuer *et al*. [25]. Moreover, as shown in fig. 5, the numerical results obtained for re-circulation length (for clear fluid), shows very good agreement with the data published by Sharma and Eswaran [26].

Results and discussion

Figure 5 shows variation of wake length *vs.* Reynolds number for the solid volume fractions of 0 (clear fluid), 0.01, 0.03, and 0.05. As shown here, the wake length increases with increasing Reynolds number. Also the wake length increases with increasing solid volume fraction because the flow separation happens earlier in nanofluid comparing with clear fluid. In nanofluid, the inertial forces in the flow field increases and these forces have significant effect on separation [17]. Therefore, separation point moves towards upstream by increasing the solid volume fraction.

Figure 6 shows the variation of bubble width *vs.* Reynolds number for different solid volume fractions. It can be seen that the bubble width increases with increasing Reynolds number for all solid volume fractions. It can also be seen that the bubble width increases with increasing solid volume fraction.

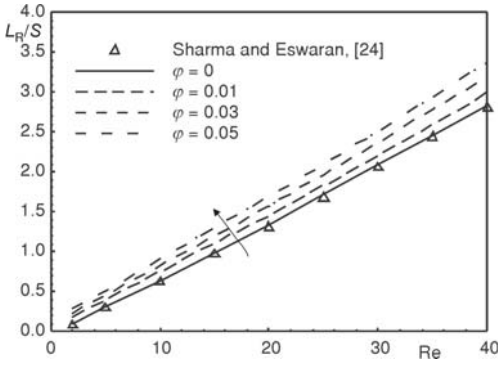

Figure 5. Variation of wake length with Re at different solid volume fractions φ

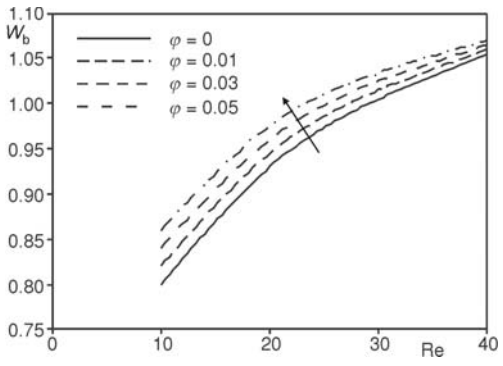

Figure 6. Variation of bubble width with Re at different solid volume fractions φ

Figure 7 shows the distribution of pressure coefficient for various solid volume fractions at the surfaces of cylinder. As shown in fig. 7, the pressure coefficient increases by increasing the solid volume fraction on sides where pressure gradient is inverse, (B-C, C-D, D-A). However, for the other side, where the pressure gradient is favorable (A-B), it shows the apposite behavior.

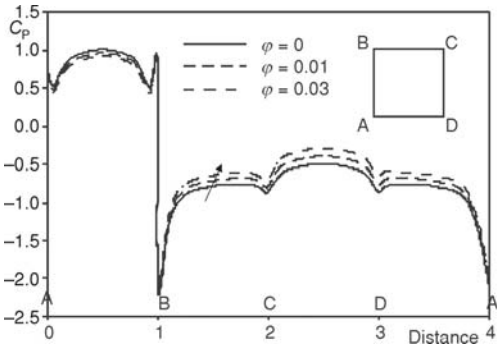

Figure 7. Distribution of pressure coefficient around surface of cylinder for various solid volume fractions φ at Re = 20

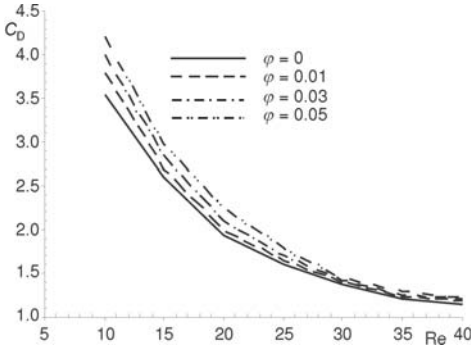

Figure 8. Variation of drag coefficient (C_D) on cylinder surface with Reynolds number at various solid volume fraction φ

The presence of nanoparticles in the fluid influences the pressure distributions on the cylinder surface [19]. The value of pressure coefficient and the pressure drop increase in adverse pressure gradient region because the inertial forces, hydrodynamic boundary layer thickness, and the viscosity increases with increasing the values of solid volume fraction [27].

The effect of nanoparticles on drag coefficient is shown in fig. 8. This figure shows that at the low Reynolds numbers, increasing the nanoparticles volume fractions significantly augments the drag coefficient. However, it does not have an important effect at high Reynolds numbers. Adding nanoparticles to the base fluid increases effective viscosity of the fluid and this increases viscous drag around the cylinder surface, thickens the hydrodynamic boundary layer, and exerts more retarding force on the shear layers. So, the drag coefficient increases by increasing solid volume fraction [19]. Note that lift coefficient is zero for our problem (Re < 40 and steady flow) because flow is symmetric about the wake centerline, which gives rise to balanced shearing and pressure forces [12, 13]. The local and average Nusselt numbers are defined as:

$$\mathrm{Nu} = -\frac{k_{\mathrm{eff}}}{k_{\mathrm{f}}}\frac{S}{T_{\mathrm{w}} - T_{\infty}}\frac{\partial T}{\partial n}\bigg|_{\text{along cylinder surface}} \tag{17}$$

$$\mathrm{Nu}_{\mathrm{ave}} = \frac{1}{A}\int_{A}\mathrm{Nu}\mathrm{d}A \tag{18}$$

where n is the direction normal to cylinder surface and A – the surface of cylinder. Also w and ∞ denotes wall and free stream, respectively.

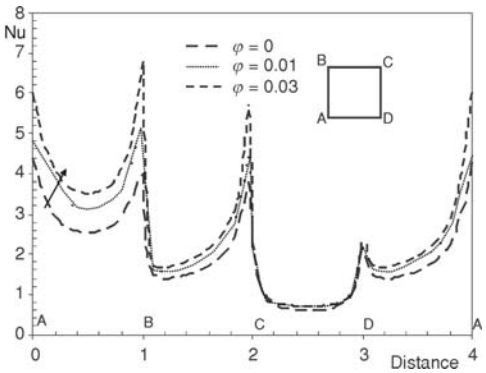

Figure 9. Distribution of local Nusselt number on surface of square cylinder at various solid volume fraction φ

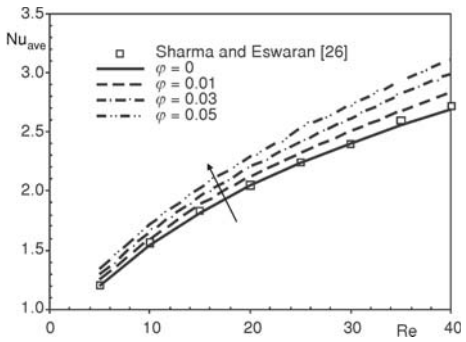

Figure 10. Variation of average Nusselt number (Nuave) on cylinder surface with Reynolds number at various solid volume fraction φ

A comparison between local Nusselt numbers for various solid volume fractions was shown in fig. 9. It shows that local Nusselt number is enhanced by adding nanoparticles to the base fluid. The data show an increase of up to 25% in convection heat transfer in A-B side as the particle volume fraction is increased to 3%.

Variation of average Nusselt number *vs*. Reynolds number for different solid volume fractions is shown in fig. 10. Figure 10 shows that increasing in both Reynolds number and solid volume fraction will increase the average Nusselt number. One of the main reasons for this behavior is Brownian motion. Note that Brownian motion of nanoparticles could contribute to the heat transfer enhancement in two ways: (1) due to motion of nanoparticles that transport heat energy, and (2) due to micro-convection of fluid surrounding nanoparticles [6].

The streamlines and isotherm contours around the cylinder were illustrated in figs. 11 and 12, for Reynolds numbers of 10, 20, and 30. Here, the contours of clear fluid and nanofluid are shown for comparison. The streamlines around the cylinder for different Reynolds numbers are shown in fig. 11. It can be seen that the re-circulation length increases as Reynolds number increases in both clear and nanofluid. However, in nanofluid the center of wake is slightly shifted away from the surface of the cylinder comparing with clear fluid. For the temperature distribution contours in fig. 12, it can be concluded that the temperature contours are steeper in the near-wake region with increasing Reynolds number. This signifies that higher Reynolds number sets a higher temperature gradient, leading to an enhanced heat transfer from the cylinder. Thus, due to higher temperature gradient, temperature contours are much denser near the front surface of the cylinder. It can also be seen from the fig. 12 that the nanofluid show higher heat transfer rate from the cylinder than clear fluid.

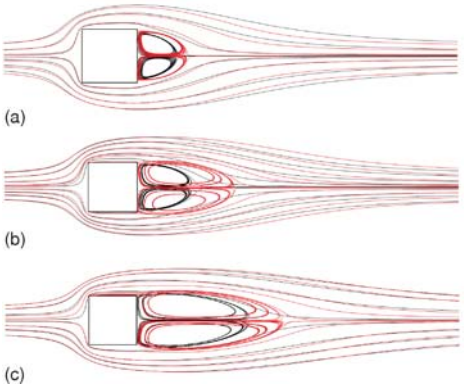

Figure 11. The streamlines around the cylinder at different Reynolds number, (black line refers to clear fluid and red line refers to nanofluid) (a) Re = 10, (b) Re = 20, (c) Re = 30

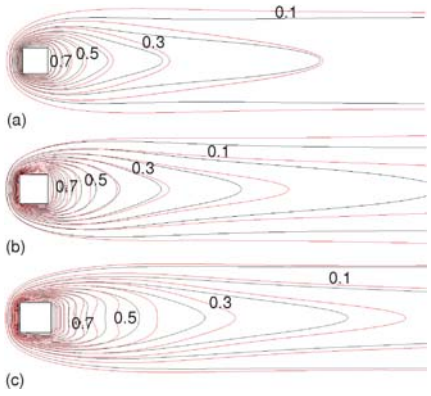

Figure 12. The isotherm contours around the cylinder at different Reynolds number, (black line refers to clear fluid and red line refers to nanofluid) (a) Re = 10, (b) Re = 20, (c) Re = 30

Conclusions

In this paper, fluid motion and heat transfer around a solid square cylinder in presence of AL_2O_3-nanoparticles has been studied numerically. Here, the effects of solid volume fraction and Reynolds number on the flow pattern and heat transfer characteristics were investigated numerically. Followings are the important results obtained from this research.

- By increasing the solid volume fraction, the magnitude of re-circulation length and bubble width will increase.
- At a Reynolds number, the local and average Nusselt numbers increases by enhancement of nanoparticles concentration.
- Pressure coefficient increases by increasing the solid volume fraction for sides where pressure gradient is inverse but for sides where the pressure gradient is favorable the pressure coefficient decreases.
- Increasing the nanoparticles volume fractions augments the drag coefficient.
- The effect of nanoparticles volume fraction on drag coefficient is significant at low Reynolds numbers.

Nomenclature

A – surface of cylinder, [m^2]
B_c – Boltzmann constant, [–]
C – specific heat, [$Jkg^{-1}K^{-1}$]
C_D – drag coefficient (= $F_D/0.5rV_{in}^2S$), [–]
C_p – pressure coefficient (= $p_\infty - pw/0.5\rho V_{in}^2$), [–]
d_f – molecular diameter of base fluid, [nm]
d_p – nano particle diameter, [nm]
F_D – drag force, [N]
h – heat transfer coefficient, [$Wm^{-2}K^{-1}$]
k – thermal conductivity of fluid, [$Wm^{-1}K^{-1}$]
LR – wake length, [m]
l_{BF} – mean free path of water, [–]
Nu – Nusselt number (= hS/k), [–]
p – pressure, [Pa]
Pe – Peclet number, (= Re×Pr), [–]
Pr – Prandtl number, (= υ_f/α_f), [–]
Re – flow Reynolds number (= $\rho_f V_{in} S/\mu_f$), [–]
S – cylinder size, [m]
T – temperature, [K]
V – velocity vector, [ms^{-1}]
W_b – bubble width, [m]
x, y – rectangular co-ordinates components, [m]

Subscripts

ave – average, [–]
B – Brownian, [–]
eff – effective, [–]
f – base fluid, [–]
in – Onlet, [–]
m – mixture, [–]
p – particle-pressure, [–]
s – solid, [–]
v – viscous, [–]
w – wall, [–]
∞ – free stream, [–]

Greek symbols

α – thermal diffusivity of fluid, [m^2s^{-1}]
δ – distance between particles, [nm]
μ – fluid dynamic viscosity, [$kgm^{-1}s^{-1}$]
υ – fluid kinematic viscosity (= μ/ρ), [m^2s^{-1}]
ρ – fluid density, [kgm^{-3}]
φ – volume fraction, [–]

References

[1] Das, S. K., *et al*., *Nanofluids: Science and Technology*, John Wiley & Sons, Hoboken, N. J., USA, 2008
[2] Lamura, A., *et al*., Multi-Particle Collision Dynamics: Flow Around a Circular and a Square Cylinder, *Euro physics Letters, 56* (2001), 3, pp. 319-325
[3] Zhou, L., *et al*., On the Specific Heat Capacity of CuO Nanofluid, *Advances in Mechanical Engineering,* (2010), Article ID 172085
[4] Peng, X. F., *et al*., Experimental Study on the Specific Heat of Nanofluids, *Journal of Materials Science & Engineering, 25* (2007), 5, pp. 719-722
[5] Wong, K. V., Castillo, M. J., Heat Transfer Mechanisms and Clustering in Nanofluids, *Advances in Mechanical Engineering*, 2010 (2010), Article ID 795478

[6] Ding, Y., *et al*., Heat Transfer Intensification Using Nanofluids, KONA *Journal of Particle and Powder, 25* (2007), pp. 23-38
[7] Ellahi, R., *et al*., Series Solutions for Magnetohydrodynamic Flow of Non-Newtonian Nanofluid and Heat Transfer in Coaxial Porous Cylinder with Slip Conditions, *J Nanoengineering and Nanosystems, 225* (2011), 3, pp. 123-132
[8] Ellahi, R., *et al*., Series Solutions of Non-Newtonian Nanofluids with Reynolds' Model and Vogel's Model by Means of the Homotopy Analysis Method, *Mathematical and Computer Modeling, 55* (2012), 7-8, pp. 1876-1891
[9] Ellahi, R., *et al*., Non Newtonian Nanofluid Flow through a Porous Medium between Two Coaxial Cylinders with Heat Transfer and Variable Viscosity, *Journal of Porous Media, 16* (2013), 3, pp. 205-216
[10] Ellahi, R., The effects of MHD and Temperature Dependent Viscosity on the Flow of Non-Newtonian Nanofluid in a Pipe: Analytical Solutions, *Applied Mathematical Modeling, 37* (2013), 3, pp. 1451-1467
[11] Dhiman, A. K., *et al*., Flow and Heat Transfer Across a Confined Square Cylinder in the Steady Flow Regime: Effect of Peclet Number, *International Journal of Heat & Mass Transfer, 48* (2005), 21-22, pp. 4598-4614
[12] Chatterjee, D., Mondal, B., Effect of Thermal Buoyancy on Vortex Shedding behind a Square Cylinder in Cross Flow at Low Reynolds Numbers, *International Journal of Heat & Mass Transfer, 54* (2011), 21-22, pp. 5262-5274.
[13] Yoon, D., *et al*., Flow Past a Square Cylinder with an Angle of Incidence, *Physics of Fluids, 22* (2010), 4, 043603
[14] Rahnama, M., *et al*., Forced Convection Heat Transfer from a Rectangular Cylinder: Effect of Aspect Ratio, *Proceedings*, 16th International Symposium on Transport Phenomena, Prague, 2005, pp. 1-5
[15] Mahmoodi, M., Mixed Convection Inside Nanofluid Filled Rectangular Enclosures with Moving Bottom Wall, *Thermal Science, 15* (2011), 3, pp. 889-903
[16] Soltanipour, H., *et al*., Numerical Analysis of Heat Transfer Enhancement with using γ-Al_2O_3-H_2O Nanofluid and Longitudinal Ribs in a Curved Duct, *Thermal Science,16* (2012), 2, pp. 469-480
[17] Valipour, M. S., Zare Ghadi, A., Numerical Investigation of Fluid Flow and Heat Transfer around a Solid Circular Cylinder Utilizing Nanofluid, *International Communications in Heat and Mass Transfer, 38* (2011), 9, pp. 1296-1304
[18] Etminan-Farooji, V., *et al*., Unconfined Laminar Nanofluid Flow and Heat Transfer around a Square Cylinder, *International Journal of Heat and Mass Transfer, 55* (2012), 5-6, pp. 1475-1485
[19] Sarkar, S., *et al*., Mixed Convective Heat Transfer of Nanofluids Past a Circular Cylinder in Cross Flow in Unsteady Regime, *International Journal of Heat and Mass Transfer, 55* (2012), 17-18, pp. 4783-4799
[20] Izadi, M., *et al*., Numerical Study of Developing Laminar Forced Convection in an Annulus, *International Journal of Thermal Sciences, 48* (2009), 11, pp. 2119-2129
[21] Zhou, S. Q., Ni, R., Measurement of the Specific Heat Capacity of Water-Based Al_2O_3 Nanofluid, *Appl. Phys. Lett, 92* (2008), 9, pp. 093-123
[22] Masoumi, N., *et al*., A New Model for Calculating the Effective Viscosity of Nanofluids, *J. Applied Physic, 42* (2009), 9, pp. 1-6
[23] Chon, C. H., *et al*., Empirical Correlation Finding the Role of Temperature and Particle Size for Nanofluid (Al_2O_3) Thermal Conductivity Enhancement, *J. Applied Physic, 87* (2005), 5, pp. 1-3
[24] Patankar, S. V., *Numerical Heat Transfer and Fluid Flow*, Hemisphere, New York, USA, 1980
[25] Breuer, M., *et al*., Accurate Computations of the Laminar Flow Past a Square Cylinder Based on Two Different Methods: Lattice-Boltzmann and Finite-Volume, *International Journal of Heat and Fluid Flow, 21* (2000), 2, pp. 186-196
[26] Sharma, A., Eswaran, V., Heat and Fluid Flow across a Square Cylinder in the Two Dimensional Laminar Flow Regime, *Numer. Heat Transfer A-Appl., 45* (2004), 3, pp. 247-269
[27] Kumar, P., Ganesan, R., A CFD Study of Turbulent Convective Heat Transfer Enhancement in Circular Pipe Flow, World Academy of Science, *Engineering and Technology, 6* (2012), 8, pp. 695-702

Paper submitted: December 24, 2012
Paper revised: April 10, 2013
Paper accepted: May 16, 2013